Sediment efflux of silicon on the Greenland margin and implications for the marine silicon cycle

Hong Chin Ng [a,*], Lucie Cassarino [a], Rebecca A. Pickering [b,c], E. Malcolm S. Woodward [d], Samantha J. Hammond[e], Katharine R. Hendry [a]

[a] School of Earth Sciences, University of Bristol, Bristol BS8 1RJ, UK.

[b] Dauphin Island Sea Laboratory, 101 Bienville Boulevard, Dauphin Island, AL 36528, USA.

[c] University of South Alabama, Mobile, AL, 36688, USA.

[d] Plymouth Marine Laboratory, Prospect Place, The Hoe, Plymouth, PL1 3DH, UK.

[e] School of Environment, Earth, and Ecosystem Sciences, The Open University, Milton Keynes, MK7 6AA, UK.

* Corresponding author: hn9381@bristol.ac.uk

Abstract

The polar region is experiencing one of the most rapid environmental changes driven by atmospheric warming, and feedbacks within the cryosphere. Under such a setting, it is crucial to understand the biogeochemical cycling of the nutrient silicon (Si) in the high latitudes, which is regulating the nutrient supply to polar ecosystems, and is linked to the global carbon cycle via diatom production. However, these efforts have been hindered by a lack of understanding of the benthic Si cycle, particularly the quantification of the sediment efflux of Si, and identification of the responsible mechanistic processes during early diagenesis. Here, we address these issues using new pore water profiles and incubation experiments on sediment cores collected from the Greenland margin and Labrador Sea, combined with Si isotope analysis and a mass balance model. Benthic Si flux at our study sites is found to be greatly heightened from values sustained by pore water molecular diffusion. The remainder of the flux is likely accountable with early dissolution of reactive biogenic silica phases at the upper sediments, and advective transport of pore waters. Our results highlight an active benthic Si cycle at a northern high-latitude continental margin, which could play a key role in recycling significant amounts of biologically available dissolved Si to the overlying water, and influencing the growth of benthic and planktonic communities in the polar region.

Keywords

Polar ocean, benthic nutrient flux, ocean silicon cycle, silicon isotopes, early diagenesis.

1. Introduction

The global biogeochemical cycle of the nutrient silicon is a process that has received widespread attention because it is coupled with the marine carbon cycle, which plays a crucial role in the

regulation of global climate. In particular, diatoms, a major phytoplankton group that builds frustules by precipitating biogenic silica (BSi) from silicic acid (H_4SiO_4), the main form of dissolved silica (DSi) in the water column, is a key modulator of the atmospheric level of primary greenhouse gas, carbon dioxide (CO_2). Diatoms are responsible for nearly half of the oceanic uptake of CO_2 (Nelson et al., 1995), and they are a fundamental component of the marine Si cycle, acting as a main sink of Si to the deep ocean and sediments (Sutton et al., 2018). However, given that seawater is undersaturated with respect to Si, over 95 % of the diatom BSi and those of other planktonic silicifiers such as radiolarians and silicoflagellates, are eventually remineralised back to DSi in the ocean (Tréguer and De La Rocha, 2013). Approximately one-third of the remineralisation occurs upon sediment deposition (Tréguer and De La Rocha, 2013), resulting in a benthic Si flux, i.e. an efflux of Si out of the sediment back to the overlying water (Frings, 2017).

Although benthic Si fluxes have been evaluated at different areas of the global ocean (Frings, 2017), a coherent explanation of its controls is yet to emerge. This is because we still lack a comprehensive understanding of the existing data to be able to provide a detailed assessment of its mechanistic processes. These processes include: molecular diffusion maintained by a DSi gradient between sediment pore waters and overlying bottom seawater (Frings, 2017), pore water mixing or advection (Janssen et al., 2005), and benthic macrofaunal activities such as bioturbation and bio-irrigation (Devol and Christensen, 1993). In addition, the magnitude of benthic Si flux further depends on the rate of dissolution of BSi in the sediment, which is governed by multiple factors including: diatom species, bacterial activity, redox condition and sediment aluminium content (Aller, 2014). Understanding benthic Si flux is an essential task before an accurate examination of the marine Si cycle can be performed, as it accounts for a major portion of the remineralisation of BSi in the ocean, which in turn contributes to the vast majority of DSi supply to

sustain the new growth of marine silicifying organisms such as diatoms (Tréguer and De La Rocha, 2013).

There have been in the past a distinct lack of benthic Si flux studies in the northern high latitudes. A recent study has highlighted that the biogeochemical cycling of Si in this region has a significant influence on the ocean Si budget (Hawkings et al., 2018). For example, physical and chemical erosion of silicate bedrock stimulated by glacial action, such as that found in Greenland, gives rise to the formation of amorphous silica (ASi) as a weathering product, which then rapidly dissolves in seawater (Hawkings et al., 2017). Melting glaciers are hence a significant source of nutrient Si that could contribute to enhancing the production of diatoms at downstream fjords and in the coastal ocean (Arrigo et al., 2017; Meire et al., 2016). There is also a diverse range of siliceous sponges found around the coasts of Canada, Greenland and in the Labrador Sea (Hendry, 2017; Murillo et al., 2018), which helps to regulate the benthic cycling of Si in the region as they utilise bottom water DSi to precipitate BSi in order to build into their skeletal elements known as spicules (Maldonado et al., 2005).

The aim of this study is to quantify the benthic Si flux coming from sediments on the Greenland continental margin and in the Labrador Sea. The approach taken here involved the acquisition of pore water profiles to estimate the molecular diffusion flux of DSi at the sediment-water interface (McManus et al., 1995), and the execution of incubation experiments (Hammond et al., 2004) on sediment cores to measure the net efflux of Si out of the sediment. Si has three stable isotopes: ^{28}Si, ^{29}Si and ^{30}Si, with their relative abundance approximately 92.2 %, 4.7 % and 3.1 % respectively. These isotopes undergo kinetic fractionation during low temperature processes such as chemical weathering, authigenic clay formation, and during biological uptake by siliceous organisms (Sutton et al., 2018). Here, the Si isotopes are employed for the first time to study

benthic Si flux in a high-latitude setting, and our results reveal new insights about the relative contribution of the multiple processes that contribute to the benthic Si flux at the study sites, along with implications for its role in the biogeochemical cycling of Si in the high latitudes.

2. Materials and methods

2.1. Study sites

During the RRS Discovery expedition DY081 (July–August 2017), seven sets of short (<0.4 m) sediment cores, DY081-MGA1 – DY081-MGA7, were collected from a range of water depths (519–3721 m) from the continental margin of South West Greenland, and also from an open ocean setting in the Labrador Sea (Fig. 1, Table 1). The sites covered a range of sediment types from fine-grained muds to coarser-grained sands, with varying degrees of bioturbation (Table 1).

The core sites are subject to the influence of glaciers to varying extents. In particular, glacial flour input (fine-grained particles generated by glacial erosion) could potentially be inferred from the uranium-series isotopes ^{224}Ra and ^{228}Th that have lithogenic origin (Hendry et al., 2019b). Elevated activity concentrations of the particle-reactive ^{228}Th (~5–10 dpm m^{-3}) observed proximal to our Greenland margin sites are consistent with the supply of glacial flour to the area (Hendry et al., 2019b). Increasing concentrations of the more soluble, short-lived ^{224}Ra (from ~1 to 9 dpm m^{-3}) along the flow path of the West Greenland Current (WGC), provides evidence for the continual addition of glacial flour to the WGC (Hendry et al., 2019b). WGC eventually mixes and subducts with other water masses to form Labrador Sea Water, providing a potential pathway for glacial flour to reach the deeper sites in the Labrador Sea (Hendry et al., 2019b).

Euphotic zone chlorophyll data (Chl *a*) obtained from DY081 expedition shows peak concentrations ranging from ~2–19 mg m^{-3} at the time of sediment core sampling, consistent with values observed during a summer phytoplankton bloom on the Greenland margin and in the Labrador Sea (Arrigo et al., 2017). Summer bloom in the region is typically associated with enhanced supply of nutrients derived from melting glaciers (Arrigo et al., 2017). There is also a spatial difference in diatom productivity in the study area. For instance, elevated diatom production rates have been observed on the western Greenland margin off Nuuk (~2–14 mmol Si m^{-2} day^{-1}), relative to the other sites (~0.1–5 mmol Si m^{-2} day^{-1}) (Hendry et al., 2019b).

Based on the remotely-operated underwater vehicle (ROV) images from cruise DY081, there is a spatial difference in the relative distribution of sponge groups in the study area. Greater abundance of hexactinellid sponges are observed at the sites in the Labrador Sea. Meanwhile, South-West Greenland margin is dominated by diverse demosponge communities, including numerous encrusting sponges (Hendry, 2017).

2.2. Field sampling

The coring device employed was a mega (multi-) coring system from UK National Marine Facilities. The system housed multiple plastic core tubes of 0.60 m length and 0.105 m internal diameter, and it was used to acquire a set of eight 'replicate' short sediment cores (<0.4 m) at each of the seven sites (MGA1–MGA7). The mega coring system was capable in preserving the sediment-water interface during sediment core collection.

One of the cores was used for pore water sampling, after the overlying core-top water was siphoned off. Rhizon filters of 0.15 µm pore size (Rhizosphere) attached to syringes were inserted into the sediment cores through holes pre-drilled on the core tube to extract filtered pore water,

generally at 0.02 m sediment depth intervals. Another replicate core was used for incubation experiments in a 4^{o} C temperature controlled cold room following the setup described in Hammond et al. (2004). The heights of the core-top water columns of MGA1–MGA7 ranged from 0.14–0.32 m at the beginning of incubations. A magnetic stirrer (one-inch long) held in a platform (open to surrounding water) at the top of incubator was set to rotate at ~33 rpm to maintain constant mixing of the water column, without resuspending the sediments. Core-top seawater was sampled and filtered through 0.45 µm at approximately every 2 hours for 24 hours. There was no observable activity of macrofaunal irrigation throughout the incubations. The pore water and core-top water samples were filtered through different pore sizes: 0.15 and 0.45 µm respectively, but a previous study suggested that these two pore sizes did not cause a significant difference in marine dissolved Si analysis (Knefelkamp et al., 2007). Samples were stored in cool, dark conditions prior to analysis, unless otherwise specified later.

Several small, pristine sponges (stalked sponge and encrusting sponges) attached on pebbles were observed atop the sediment column of MGA5 upon core retrieval (Appendix Fig. A.1). They remained inside the core tube until the end of incubation experiment. The sponges were then retrieved and preserved in 95 % ethanol and stored in a freezer at -20^{o} C for subsequent Si isotope analysis (Section 2.4).

2.3. Measurement of dissolved Si concentrations, [DSi]

Pore water [DSi] was measured on-board and post-expedition in the University of Bristol with molybdate-blue method (Strickland and Parsons, 1968) using a V-1200 Vis spectrophotometer. Following the GO-SHIP procedures in Hydes et al. (2010), split portions of core-top water samples were frozen at -20^{o} C immediately after sampling. Prior to [DSi] measurements, samples were defrosted in a warm water bath for 45 minutes, followed by equilibration to room temperature for

30–40 minutes. Core-top water [DSi] was analysed at the Plymouth Marine Laboratory using a SEAL analytical AAIII segmented flow colorimetric auto-analyser, as described in Woodward and Rees (2001). Seawater certified nutrient reference materials (KANSO Technos Ltd. Japan) were measured during the analysis to monitor analyser performance and to ensure quality control of the final data. The analytical errors associated with the two methods above were 2–3 %.

2.4. Si isotope analysis

A clean laboratory sample preparation technique for pore water and core-top waters, prior to instrumental analysis, involved the pre-concentration of Si using a Mg-induced co-precipitation method broadly following Souza et al. (2012). Briefly, $Mg(OH)_2$ was precipitated by adding 1 M NaOH (Titripur® Reag. Ph Eur grade) to the pH neutral samples in two steps. Precipitates were washed by adding 0.001 M NaOH, centrifuging, and removing the supernatant three times, so as to quantitatively remove excess cations and anions (mainly Na^+, Cl^-, SO_4^{2-}, Ca^{2+} and K^+). The final precipitates were then dissolved with 6 M in-house distilled HCl from the Bristol Isotope Group laboratory, and the resulting solutions were diluted with 18.2 MΩ Milli-Q water for subsequent column chemistry.

Sample preparation method for the sponges were mainly based on Hendry et al. (2019a). Milli-Q rinsed, air-dried sponge subsamples were cleaned with 30 % reagent grade H_2O_2, initially at room temperature, then in two steps at 80° C in a water bath, with Milli-Q rinses in between. Further cleaning of the sponges was carried out with concentrated HNO_3 (in-house distilled) followed by a Milli-Q rinse, three times, before drying on a hotplate. Dry sponge spicules were weighed, and a final HNO_3 clean was carried out, before drying. The spicules were then dissolved with 0.4 M NaOH (Titripur® Reag. Ph Eur grade) on a hotplate at 100° C for 3 days.

188 The processed pore water, core-top water and dissolved sponge samples were passed through
189 cation exchange columns following the procedures of Georg et al. (2006), purifying the solution
190 prior to instrumental analysis. Briefly, polypropylene columns were filled with 1.8 ml Bio-Rad
191 AG50W-X12, 200-400 mesh cation exchange resin in H^+ form, which were rinsed with in-house
192 distilled HCl and Milli-Q before the samples were loaded onto the columns. Milli-Q was then used
193 to elute any sample remaining in the column, resulting in final elutions of 3–4 ml of 1–2 ppm Si
194 solution.
195
196 Measurements of the Si isotopes (^{28}Si, ^{29}Si, ^{30}Si) were carried out at the Bristol Isotope Group
197 laboratory using a Thermo-Finnigan Neptune, multi collector-inductively coupled plasma-mass
198 spectrometer (MC-ICP-MS), where samples were introduced into the plasma using a CETAC PFA
199 spray chamber (wet plasma) and PFA nebuliser (100 ul min^{-1}). The MC-ICP-MS operating
200 conditions followed Hendry et al. (2016). For pore water and core-top water samples, solutions
201 were doped with H_2SO_4 (ROMIL UpA^{TM}) and HCl (in-house distilled) to reach the target excess
202 concentrations of 500 ppm for SO_4^{2-} and 3,500 ppm for Cl^- in order to alleviate the anionic matrix
203 effects (Hughes et al., 2011). Corrections for both instrumental mass bias and matrix effects were
204 carried out using standard-sample bracketing and Mg-doping methods (Cardinal et al., 2003).
205
206 Si isotope composition of a given material is typically expressed as $\delta^{30}Si$ values relative to the
207 international standard NBS-28 per mil (‰):

208 $$\delta^{30}\mathrm{Si} = \left[\frac{\left(^{30}\mathrm{Si}/^{28}\mathrm{Si}\right)_{\mathrm{sample}}}{\left(^{30}\mathrm{Si}/^{28}\mathrm{Si}\right)_{\mathrm{NBS-28}}} - 1\right] \times 1000 \quad (1)$$

209 Replicate measurements of several reference standards (Table 2) were carried out to assess long-
210 term external reproducibility of the protocol, and the mean $\delta^{30}Si$ obtained for the standards agree
211 with published values within 2 SD (Table 2). Some replicate measurements were made on five

pore water samples (n = 2–3) (Fig. 2b, d & f), five core-top water samples (n = 2–3) (Fig. 3b), and the sponge samples (n = 2–4) (Appendix data). The range of 2 SD obtained in these sample replicate measurements are 0.06–0.28 ‰ for pore water, 0.0003–0.19 ‰ for core-top water, and 0.14–0.25 ‰ for sponge. The $\delta^{29}Si$ and $\delta^{30}Si$ values of all standards and samples measured during this study plot on a straight line (Appendix Fig. A.2) through the origin with a gradient of 0.5181 ± 0.0040, which lies between thermodynamic (0.5210) and kinetic (0.5105) mass-dependent fractionation (Cardinal et al., 2003).

2.5. Pore water dissolved major and trace element concentration measurement

Split portions of pore water samples were acidified by adding 1 % v/v 10 M in-house distilled HCl, and were left to equilibrate for at least three months prior to dissolved concentration measurements of selected elements. Major elements: [K] and [Mg] were analysed with inductively coupled plasma-optical emission spectroscopy (ICP-OES) using an Agilent 710 instrument at the University of Bristol. Trace elements: [Al], [Fe], and [Mn] were analysed using an Agilent 8800 inductively coupled plasma-triple quadrupole-mass spectrometer (ICP-QQQ-MS) at the Open University. Monitoring of analyser performance was carried out on both instruments with periodic measurements of blanks and calibration standards. Data quality of the low concentration trace elements was further constrained with the analysis of a river water (SLRS-6) and a nearshore seawater (CASS-6) certified reference material. [Al], [Fe] and [Mn] measurements of these reference standards agree well with certified values within 95 % confidence interval.

2.6. Calculation of benthic Si flux

Benthic flux of Si from the sediment to the overlying bottom water at each study site was evaluated using two methods: (1) pore water [DSi] profile, and (2) core-top water [DSi] from the incubation experiment. Molecular diffusion flux, $J_{diffusion}$ (mmol m^{-2} day^{-1}), through the sediment-

water interface was estimated by combining Fick's First Law of Diffusion, and exponential fitting of the pore water [DSi] profile (McManus et al., 1995) (Fig. 2a, c, & e):

$$J_{diffusion} = \phi_0 \times (D_m/\theta^2) \times \beta \times (C_d - C_0) \quad (2)$$

$$C_z = C_d - (C_d - C_0) \times e^{-\beta z} \quad (3)$$

ϕ_0 is the core-top sediment porosity; θ^2 is the tortuosity; D_m (m^2 day^{-1}) is the molecular diffusion coefficient for silicic acid in free solution; β (m^{-1}) expresses the curvature of the exponential profile, which reflects the depth at which pore water DSi approaches asymptotic concentrations, C_d (mmol m^{-3}); C_0 (mmol m^{-3}) is the ambient core-top water [DSi]; C_z (mmol m^{-3}) is pore water [DSi] at a given sediment core depth, z (m).

The values of the parameters used to calculate $J_{diffusion}$ for MGA1–MGA7 are listed in Table 3, and the uncertainties associated with $J_{diffusion}$ was propagated from all analytical errors (Table 3). The potential presence of a diffusive boundary layer at the sediment-water interface, typically possessing a thickness of 0.2–1 mm (Schulz and Zabel, 2006), was not explicitly accounted for. This might cause minor underestimation of C_0, and might therefore lead to slight overestimation of the calculated $J_{diffusion}$ (McManus et al., 1995), but the effect was expected to be small relative to the uncertainties associated with the other parameters (Table 3) used to derive $J_{diffusion}$ (McManus et al., 1995).

The apparent total benthic Si flux, J_{total}, was evaluated based on the rate of change of core-top water [DSi] in the core incubation (Hammond et al., 2004). During the incubation, the height of the core-top water column, h, decreased after each sampling interval. The decrease in h led to systematic bias in the rate of change of core-top water [DSi] (Hammond et al., 2004). Correction for this bias was made by fitting a linear regression to a plot of measured core-top water [DSi] (mmol m^{-3}) against the ratio of incubation time to h, t/h (day m^{-1}) (Hammond et al., 2004) (Fig. 3c).

The slope of the regression was J_{total} (mmol m^{-2} day^{-1}), and the uncertainty associated with J_{total} was directly derived from the error of the slope (Fig. 3c).

The flux calculations above were not corrected for temperature effects on adsorption/desorption of Si onto sediment particles or dissolution rates of BSi (Hammond et al., 2004). This was because core incubations were carried out at a temperature close to those of in-situ bottom water at the core sites (2–4^{o} C). Sampling of pore waters were carried out at room temperature, but they were done within 10 hours of sediment core retrievals, which was a timeframe where no critical change in pore water [DSi] profile was observed, as shown in a previous experiment (Hendry et al., 2019b).

3. Results and Discussion

3.1. Pore water data and early diagenesis of Si

Pore water [DSi] data from MGA1–MGA7 have been presented elsewhere (Hendry et al., 2019b). Overall, pore water [DSi] and $\delta^{30}Si$ observed here range from 76 to 616 mmol m^{-3} (unit equivalent to µM) and +0.76 to +2.08 ‰ respectively. The down-core trends of pore water [DSi] at all of our sites could generally be described with exponential profiles, where [DSi] broadly increases with increasing core depths at ever decreasing rates towards asymptotic values (Fig. 2a, c & e).

The pore water profiles of [DSi] and $\delta^{30}Si$ reflect early diagenesis of Si that is occurring in the marine sediments. For instance, the observed increases in pore water [DSi] (Fig. 2a, c & e) are primarily associated with dissolution of reactive silica phases (Aller, 2014). The pore water Si isotope data might provide further insights on some of the more distinct constituents: diatom BSi, sponge BSi, and glacial ASi, that all contribute to the increases in pore water [DSi], based on their

different isotopic compositions. The diatom BSi at our study sites is expected to have relatively high $\delta^{30}Si$: broadly greater than +1.5 ‰, following existing measurements in the northern high-latitude ocean (Varela et al., 2016). Indication of high DSi utilisation in the study area is supported by a recent study, which has found active diatom production that consumes around 4–10 % of the euphotic zone DSi inventory daily (Hendry et al., 2019b). Such high DSi utilisation provides further evidence for relatively positive diatom $\delta^{30}Si$ at our sites, given the progressive enrichment of ^{30}Si in the euphotic zone DSi inventory utilised for BSi formation (de la Rocha et al., 1997). In contrast, sponge BSi has lighter $\delta^{30}Si$, mainly less than 0 ‰ (Hendry et al., 2019a), while the glacial ASi has been recently found to have $\delta^{30}Si$ in the range of -0.5 to -0.2 ‰ (Hatton et al., 2019; Hawkings et al., 2018).

MGA6 and MGA4 generally exhibit down-core decreases in pore water $\delta^{30}Si$ towards values lowest at +0.76 ‰ (Fig. 2f) and +1.05 ‰ (Fig. 2d) respectively, and at MGA7 pore water $\delta^{30}Si$ is evidently reduced (+1.10 to +1.26 ‰) relative to its overlying core-top water (+1.58 ‰) (Fig. 2f). Assuming there is no Si isotope fractionation during BSi/glacial ASi dissolution, these observations potentially reflect a relative increase in the dissolution of endmembers with the lighter Si isotope composition: sponge BSi and glacial ASi in MGA4, MGA6 and MGA7. In contrast, pore water $\delta^{30}Si$ in MGA1, MGA2, MGA3 and MGA5 are elevated overall relative to their overlying core-top water values, and are generally at around or higher than +1.5 ‰ (Fig. 2b, d & f), which are in the range of $\delta^{30}Si$ of diatom BSi inferred for the core sites. Therefore, dissolution of diatom BSi might have contributed to the pore water $\delta^{30}Si$ observations in these four cores.

A previous study has shown some evidence of reverse weathering in Arctic sediments (März et al., 2015). Reverse weathering generally refers to the formation of authigenic clays from (dissolving) BSi, reactive Al and Fe (oxyhydroxides or their dissolved forms), and major cations dissolved in

311 pore water especially K and Mg (Aller, 2014; Michalopoulos and Aller, 2004). Precipitation of
312 authigenic clays has been suggested to preferentially incorporate the lighter Si isotopes resulting
313 in a heavier isotopic composition in the pore water (Ehlert et al., 2016).
314
315 Combined pore water $\delta^{30}Si$ and elemental concentration data might provide an indication of
316 reverse weathering taking place in some of our cores. For example, strong down-core reductions
317 of pore water [K] and [Mg] observed in MGA5 (Fig. 4c) are consistent with uptake of the dissolved
318 cations by reverse weathering. MGA5 pore water [DSi] and $\delta^{30}Si$ profiles (Fig. 2e & f) might be
319 reflecting a balance between multiple diagenetic processes, including reverse weathering and
320 BSi/glacial ASi dissolution. Peaks of pore water [Al] observed (up to 3.2 mmol m^{-3}) from ~0.15–0.30
321 m core depth of MGA3 (Fig. 4b) might suggest increased availability of reactive Al, which could
322 enhance rates of reverse weathering. This is in agreement with pore water $\delta^{30}Si$ increase (Fig. 2d)
323 and [Mg] decrease (Fig. 4b) observed at the same MGA3 core depth interval. However, a
324 corresponding pore water [K] decrease is not observed (Fig. 4b), perhaps implying the formation
325 of authigenic clays that differ from the typical reverse weathering reactions shown in previous
326 studies (Aller, 2014; Michalopoulos and Aller, 2004).
327
328 Diagenesis of Si has also been linked to sediment redox conditions, mainly via oxidative-
329 precipitation and reductive-dissolution of Fe oxyhydroxides (Aller, 2014). Overall, elevated levels
330 of pore water [Fe] (up to 72 mmol m^{-3}) in MGA3–MGA6 (Fig. 4) are indicative of bacteria-mediated
331 reductive dissolution of Fe oxyhydroxides, reflecting anoxic conditions in these cores (Aller, 2014).
332 Down-core decrease in MGA4 pore water [Fe] (Fig. 4b) most likely is associated with the
333 precipitation of reduced Fe forming iron sulphides (Aller, 2014). Interestingly, MGA3–MGA6 also
334 exhibit overall higher levels of pore water [DSi] than the other cores (Fig. 2a, c & e). This
335 observation is consistent with both desorption of Si from Fe oxyhydroxide following its reductive

dissolution, and increased BSi solubility after losing Fe oxyhydroxide coatings in anoxic sediments, lending support to the role of sediment Fe cycling in regulating pore water [DSi] (Aller, 2014). However, there is no obvious link between the MGA cores' pore water [Fe] (Fig. 4) and $\delta^{30}Si$ (Fig. 2b, d & f) profiles, suggesting that redox-driven sediment Fe cycling might not have imposed a clear Si isotope signal on the pore waters compared to the other diagenetic activities.

Our pore water results have shown a mix of diagenetic processes that play a role in regulating pore water DSi (and $\delta^{30}Si$), which include dissolution of diatom BSi, sponge BSi and glacial ASi, reverse weathering, and redox cycling of Fe. Marine silicate weathering is also a potential process that might supply DSi to the pore water (Tréguer and De La Rocha, 2013). The net effects of these processes are the exponential pore water [DSi] profiles (Fig. 2a, c & e), which give rise to molecular diffusion fluxes that contribute to the net effluxes of Si out of the sediments into the overlying seawater. These diffusion fluxes will carry distinct Si isotopic signatures imposed by the multiple diagenetic processes described above.

3.2. Core incubation results and rapid sponge dissolution

All core-top water [DSi] concentrations, over the entire incubation period, range from 6.8 to 24.7 mmol m^{-3}. The core-top water [DSi] exhibits a linear increase with time in all incubation experiments (Fig. 3a), indicating net positive effluxes of Si out of the sediment into the overlying bottom water at all study sites, regardless of water depths or marine settings. Whilst the relative trends through time are consistent, there is a significant variation in the absolute gradient of core-top water [DSi] increase against incubation time between the core locations (Fig. 3a). Such variation reflects a spatial difference in the magnitude of sediment efflux of Si in the study area, and this is further evaluated in Section 3.3.

MGA1, MGA2, MGA4 and MGA7 display minor changes in core-top water $\delta^{30}Si$ over the incubation period. Both MGA3 and MGA6 core-top waters show gradual but statistically significant ($p<0.05$) linear increases in $\delta^{30}Si$ from +1.29 to +1.66 ‰, and +1.36 to +1.55 ‰ respectively, during the incubation experiment (Fig. 3b). The gradual $\delta^{30}Si$ increase likely reflects continual dissolution of diatom BSi (which likely has $\delta^{30}Si$ signature of greater than +1.5 ‰ for our sites, see Section 3.1) at the uppermost sediment layers of MGA3 and MGA6. Contrary to the above, MGA5 core-top water exhibits a pronounced decrease in $\delta^{30}Si$ from +1.27 to +0.18 ‰ during the incubation (Fig. 3b).

One stalked sponge and four encrusted sponges found attached on pebbles atop the sediment column of MGA5 show average $\delta^{30}Si$ ranging between -1.02 and -1.45 ‰ (Fig. 3b). The significant decrease of MGA5 core-top water $\delta^{30}Si$ towards observed sponge values, along with the considerable increase of its [DSi] (Fig. 3) are indicative of substantial remineralisation of the sponge individuals that were found atop the sediment column at this South West Greenland site, even before sediment burial. Our results suggest that under certain conditions sponge spicules have considerable dissolution rates, contrary to the findings of a previous study (Maldonado et al., 2005), which showed no detectable dissolution of sponge spicules for at least 14 days. This discrepancy could be related to the spicule structure, spicule size or the degree of sponge silicification (Bertolino et al., 2017; Conley and Schelske, 1993). The more lightly silicified encrusting sponges, and the stalked sponge presented here, might have structural properties that are more susceptible to dissolution than sponges that have been previously investigated (Maldonado et al., 2005).

Overall, sponges act as a net sink of Si through the precipitation of BSi from bottom water DSi to build spicules, which are subsequently buried in the sediments (Tréguer and De La Rocha, 2013). However, these new results highlight the significance of sponge BSi remineralisation even prior to

sediment burial, which suggests that spicule dissolution could be a net contributor to benthic Si flux in certain continental margin settings. Our findings also imply that spicule dissolution rates may vary between different sponge species (Bertolino et al., 2017), in addition to the variation in their DSi uptake rates during growth (López-Acosta et al., 2018).

3.3. Benthic Si flux processes

Based on the pore water [DSi] profiles, the estimated molecular diffusion fluxes of Si, $J_{diffusion}$, for MGA1–MGA7, across the sediment-water interface, range between 0.06 and 0.32 mmol m^{-2} day^{-1}. In contrast, the total effluxes of Si from the sediment into the overlying bottom water, J_{total}, when directly measured from the core incubation experiments, are larger in magnitude (Fig. 5). There is a substantial variation in J_{total} across the study sites, ranging between 0.31 and 3.08 mmol m^{-2} day^{-1}. Using the calculated fluxes, a mass balance of benthic Si flux can be developed for our study sites:

$$J_{total} = J_{diffusion} + (J_{sponge}) + J_{residual} \quad (4)$$

$J_{residual}$ is defined as the residual benthic Si flux that is not accounted for by $J_{diffusion}$, and pre-burial sponge dissolution, J_{sponge}, for MGA5. For all the other sites, $J_{residual}$ is derived by subtracting $J_{diffusion}$ from J_{total} at each site, and this ranges between 0.13 and 1.74 mmol m^{-2} day^{-1} (Table 4). For MGA5, we assume that $J_{residual}$ is similar to nearby sites: MGA6 and MGA7, and the benthic flux associated with J_{sponge} is then estimated by subtracting $J_{diffusion}$ and the inferred $J_{residual}$ from the J_{total} of the site. J_{sponge} at MGA5 is found to be 2.53 mmol m^{-2} day^{-1} (Table 4).

Rapid remineralisation of BSi in the uppermost sediment layer coupled with a non-steady state condition in the pore water (Schulz and Zabel, 2006) is a likely contributing factor to $J_{residual}$. The sediment cores were collected during the summer bloom period (Section 2.1). The pore water

[DSi] profiles might not have sufficient time to respond to the recent enhanced deposition of fresh diatom BSi from the summer bloom, giving rise to the offset between the pore water-derived $J_{diffusion}$ and core incubation-derived J_{total}. Rapid remineralisation of freshly deposited BSi might be consistent with the overall low sediment BSi(/ASi) content (0.04–0.56 weight %) observed in several cores: MGA2, MGA3, MGA5, MGA6 and MGA7 (Appendix Fig. A.3). In addition, it might be possible for the stirring of core-top water column during the incubation experiment (Section 2.2) to drive movement of water through permeable upper sediments (Janssen et al., 2005), such as those in MGA2 and MGA3 that are mainly composed of sandy sediment (Table 1). If true, the resulting pore water advection might lead to a net transport of Si to the overlying water column, contributing to $J_{residual}$ in these two cores.

Further evaluation on the multiple processes that constitute benthic Si flux can be carried out by constructing the isotopic mass balance, which assumes no Si isotope fractionation during BSi/glacial ASi dissolution:

$$\frac{d(C\cdot\delta^{30}Si_{core-top\ water})}{d(t/h)} = J_{diffusion}\cdot\delta^{30}Si_{diffusion} + \left(J_{sponge}\cdot\delta^{30}Si_{sponge}\right) + J_{residual}\cdot\delta^{30}Si_{residual} \quad (5)$$

$\frac{d(C\cdot\delta^{30}Si_{core-top\ water})}{d(t/h)}$ (values in Table 4) is the derivative of the product between core-top water [DSi] and its isotopic composition with respect to the t/h parameter (definition in Section 2.6). The shallowest available pore water $\delta^{30}Si$ is used as an approximate representation of $\delta^{30}Si_{diffusion}$, the isotopic signature associated with molecular diffusion flux (Table 4). $\delta^{30}Si_{sponge}$ is the average isotope composition of sponges found atop the sediment column of MGA5 (Table 4). This equation could be used to estimate $\delta^{30}Si_{residual}$, which represents the integrated isotopic signature of the endmember(s) responsible for $J_{residual}$. The isotopic mass balance has not accounted for back diffusion of core-top water DSi into sediment pore water, but the effect should be minimal given the much lower [DSi] in core-top water.

The calculated $\delta^{30}Si_{residual}$ for MGA1, MGA2, MGA3, MGA4, MGA6 and MGA7 range between +1.47 and +1.76 ‰ (Table 4). If $J_{residual}$ is mainly attributed to the rapid remineralisation of freshly deposited diatom BSi (with non-steady state condition in pore water), then $\delta^{30}Si_{residual}$ might largely reflect the isotopic signature of diatom BSi. The $\delta^{30}Si_{residual}$ of MGA2 and MGA3 might also have some mixed isotopic signals advected from pore waters in the permeable upper sediments. For MGA5, the calculated $\delta^{30}Si_{residual}$ (+2.71 ‰) is evidently higher than the other sites (Table 4), which might imply the influence of sea-ice diatoms that could have heavy Si isotope composition (Varela et al., 2016). Alternatively, such a difference might be attributed to the underestimation of $J_{residual}$ at MGA5, which has been assumed to be similar to MGA6 and MGA7; and to the potential of rapid authigenic clay formation in the upper sediments.

Spatial variation in benthic Si flux between the study sites can be seen more clearly with the isotopic mass balance model. The highest flux recorded at MGA5 (3.08 mmol m^{-2} day^{-1}) is largely (~82 %) due to rapid dissolution of sponges (Fig. 5, Table 4). The second largest flux is observed in a core from the western Greenland margin: MGA3 (1.87 mmol m^{-2} day^{-1}) (Fig. 5, Table 4), with a significant portion of it possibly attributed to remineralisation of seasonally intensified diatom BSi deposition at the uppermost sediment layer. This is potentially consistent with the higher diatom production rates (~2–14 mmol Si m^{-2} day^{-1}) found in the vicinity of MGA3 core site (Hendry et al., 2019b). Our results also open the possibility for pore water advection (through permeable upper sediments) to contribute to benthic Si flux in core MGA2 and MGA3, not just in incubation experiment, but also under natural environmental condition. This is because pore water advection could be caused by horizontal advection of bottom currents over uneven sediment surface (Janssen et al., 2005; Schulz and Zabel, 2006), and active bottom currents are potentially present on the Greenland margin (Hendry et al., 2019b) and in the Labrador Sea (Handmann et al., 2018).

Sediment bio-irrigation is another process that could contribute to benthic Si flux, as burrowing macrofauna could flush DSi-enriched pore water to the overlying seawater (Devol and Christensen, 1993; Hammond et al., 2004). This process was likely under-represented in our core incubation, where minimal benthic macrofaunal activity was observed.

3.4. New interpretations of benthic Si flux in northern high latitudes, and the global ocean

We have produced a new compilation of global benthic Si flux to include our data (Fig. 6). This compilation is more inclusive than previously reported (Frings, 2017), as we also include direct measurements of total benthic Si fluxes, J_{total} (Fig. 6b), with the core incubation and benthic chamber methods (Hammond et al., 2004), in addition to diffusive benthic Si fluxes, $J_{diffusion}$ (Fig. 6a) (Frings, 2017). $\Delta J_{total\text{-}diffusion}$, the difference between J_{total} and $J_{diffusion}$, have also been calculated when both values have been evaluated at the same or proximal sites (<15 km distance apart). Overall, we find a range of $\Delta J_{total\text{-}diffusion}$ from -0.8 to +13.5 mmol m^{-2} day^{-1} (Fig. 6c). The mechanisms proposed to explain our results from the Greenland margin and Labrador Sea might also contribute to the interpretation of the global $\Delta J_{total\text{-}diffusion}$ observations.

For instance, non-steady state condition in pore water arised from seasonal variation in BSi deposition might lead to either positive or negative $\Delta J_{total\text{-}diffusion}$ at different times of the year(s) (Schulz and Zabel, 2006), and might explain some of the observed range above (Fig. 6c). Alternatively, sites with negative fluxes might reflect increased rates of benthic DSi removal by processes such as sponge uptake and authigenic clay formation. Interestingly, some of the highest J_{total} and $\Delta J_{total\text{-}diffusion}$ are consistently observed at continental margins (Fig. 6b & c), including those proximal to estuarine and deltaic settings, where rapid rates of reverse weathering are expected (Tréguer and De La Rocha, 2013). Further explanation of these observations might rely on other non-diffusive processes. For example, there could be: increased sediment bio-irrigation (Devol and

484 Christensen, 1993) at productive margins due to greater abundance of burrowing benthic
485 organisms, enhanced pore water advection in continental shelf sediments that are subjected to
486 high energy bottom currents (Janssen et al., 2005), and pre-burial rapid dissolution of certain
487 sponge group. Our compilation highlights that benthic Si flux is not solely maintained by diffusion
488 of pore water DSi at certain settings, which has important implications for existing evaluations of
489 the oceanic Si budget that have implicitly made such an assumption (Frings, 2017; Tréguer and De
490 La Rocha, 2013).
491
492 Our compilation also reveals that the benthic Si flux observed at the high-latitude continental
493 margins is relatively significant in magnitude – generally larger than the open ocean sites, though
494 smaller than the low-latitude marginal sites (Fig. 6b). Strong benthic fluxes might be particularly
495 important for the western Greenland margin, where wind-driven coastal upwelling takes place.
496 Previous studies provide some indications that episodes of northerly wind events in this region
497 (Dumont et al., 2010; Hvid Ribergaard et al., 2004) could upwell waters from hundreds of meters
498 depths (Dumont et al., 2010), which potentially cover the depth range of western Greenland
499 continental shelf (<725 m) (Gougeon et al., 2017). Therefore, sediment efflux of Si from western
500 Greenland shelf could get entrained in the upwelling water mass and become a source of this
501 nutrient to the coastal surface ocean. The range of J_{total} (Fig. 5) derived from our continental shelf
502 sites (Fig. 1) MGA4 and MGA5 might provide a preliminary estimate of benthic Si flux from the
503 western Greenland shelf. Given the region's approximate area of 0.24 Tm^2 (from 75–60^o N, with
504 shelf break depth of ~200–700 m (Gougeon et al., 2017)), total sediment efflux of Si from western
505 Greenland shelf is estimated to be 0.15 (0.04–0.27) Tmol $year^{-1}$. This is in the same order of
506 magnitude as the continental inputs of Si in the northern high latitudes – previous estimates of
507 total Si export from Greenland Ice Sheet and the pan-Arctic rivers are 0.2 and 0.35 Tmol $year^{-1}$
508 respectively (Hawkings et al., 2017).

Based on the estimation above, benthic flux is most likely a significant source of nutrient Si that contributes to sustaining both the diverse (benthic) sponge communities (Hendry, 2017), and the enhanced levels of (planktonic) diatom productivity (~2–14 mmol Si m^{-2} day^{-1}) (Hendry et al., 2019b) observed at the western Greenland margin. Interestingly, surface water [DSi] of the region is very low (<5 mmol m^{-3}) (Hendry et al., 2019b). These combined observations support the notion of a rapid and highly-tuned pelagic-benthic recycling of Si on the Greenland margin, where sediment efflux might be supplying the remineralised nutrients back to the deep and surface ocean, which are then rapidly utilised through new sponge and phytoplankton growth. Similar processes might take place at other coastal upwelling sites in the Arctic region, and the proposed scenario is consistent with the presence of active biogeochemical cycling of Si in the northern high-latitude ocean margins.

4. Conclusions

The pore water [DSi] and δ^{30}Si data from the Greenland margin and Labrador Sea reflect a mix of diagenetic activities, which include: the dissolution of diatom BSi, sponge BSi and glacial ASi, reverse weathering, and the redox cycling of Fe. The net effects of these processes are the exponential pore water [DSi] profiles which give rise to molecular diffusion fluxes. However, the core incubation data suggests that diffusion flux alone could not account for the total sediment efflux of Si to the overlying water column. Using our new data, we present the first Si isotope mass balance model, which is a potential tool for the identification and evaluation of the nature and relative magnitude of the different processes that contribute to benthic Si flux in a glaciated environment. Results provide supporting evidence for multiple mechanisms that could contribute to the remainder of benthic Si fluxes at our high-latitude sites. These mechanisms include: pre-burial rapid dissolution of certain sponge group, seasonally intensified deposition of fresh diatoms

in the uppermost sediments coupled with a non-steady state condition in pore water, and pore water advection. This study also reveals that the benthic Si fluxes at the northern high-latitude continental margins are overall higher than those in the open ocean. In particular, we find that strong benthic fluxes are likely recycling substantial amounts of Si to sustain new sponge and phytoplankton growth at the western Greenland margin, lending support to the presence of active biogeochemical cycling of Si in the northern high-latitude ocean margins.

Acknowledgements

This work was supported by the European Research Council project ICY-LAB (grant number 678371). We would like to express our gratitude to the scientists and crew of RRS Discovery (expedition DY081) for their assistance in sample collection. In particular, we thank George Rowland and Allison Jacobel for their help with pore water acquisition and core incubation experiments, and Claire Goodwin for sponge identification. We appreciate the help of Christopher D. Coath in maintaining the operation of the Thermo-Finnigan Neptune MC-ICP-MS in the Bristol Isotope Group laboratory. We also thank students from the University of Bristol: Georgia Gullick, Phooi Yee Tang, Kaelin Holloway and Rachael Ward for their assistance in sample preparation and analysis.

References

Aller, R.C., 2014. Sedimentary Diagenesis, Depositional Environments, and Benthic Fluxes, in: Holland, H.D., Turekian, K.K. (Eds.), Treatise on Geochemistry, Second Edition, vol. 8. Elsevier, Oxford, pp. 293-334.

Arrigo, K.R., Dijken, G.L., Castelao, R.M., Luo, H., Rennermalm, Å.K., Tedesco, M., Mote, T.L., Oliver, H., Yager, P.L., 2017. Melting glaciers stimulate large summer phytoplankton blooms in southwest Greenland waters. *Geophys Res Lett* **44**, 6278-6285.

Bertolino, M., Cattaneo-Vietti, R., Pansini, M., Santini, C., Bavestrello, G., 2017. Siliceous sponge spicule dissolution: In field experimental evidences from temperate and tropical waters. *Estuarine, Coastal and Shelf Science* **184**, 46-53.

Boudreau, B.P., 1996. The diffusive tortuosity of fine-grained unlithified sediments. *Geochim Cosmochim Ac* **60**, 3139-3142.

562 Cardinal, D., Alleman, L.Y., de Jong, J., Ziegler, K., André, L., 2003. Isotopic composition of silicon measured by
563 multicollector plasma source mass spectrometry in dry plasma mode. *Journal of Analytical Atomic Spectrometry* **18**,
564 213-218.

565 Conley, D.J., Schelske, C.L., 1993. Potential role of sponge spicules in influencing the silicon biogeochemistry of Florida
566 lakes. *Canadian Journal of Fisheries and Aquatic Sciences* **50**, 296-302.

567 de la Rocha, C.L., Brzezinski, M.A., DeNiro, M.J., 1997. Fractionation of silicon isotopes by marine diatoms during
568 biogenic silica formation. *Geochim Cosmochim Ac* **61**, 5051-5056.

569 Devol, A.H., Christensen, J.P., 1993. Benthic fluxes and nitrogen cycling in sediments of the continental margin of the
570 eastern North Pacific. *Journal of Marine Research* **51**, 345-372.

571 Dumont, D., Gratton, Y., Arbetter, T.E., 2010. Modeling Wind-Driven Circulation and Landfast Ice-Edge Processes
572 during Polynya Events in Northern Baffin Bay. *J Phys Oceanogr* **40**, 1356-1372.

573 Ehlert, C., Doering, K., Wallmann, K., Scholz, F., Sommer, S., Grasse, P., Geilert, S., Frank, M., 2016. Stable silicon
574 isotope signatures of marine pore waters – Biogenic opal dissolution versus authigenic clay mineral formation.
575 *Geochim Cosmochim Ac* **191**, 102-117.

576 Frings, P., 2017. Revisiting the dissolution of biogenic Si in marine sediments: a key term in the ocean Si budget. *Acta*
577 *Geochimica* **36**, 429-432.

578 Georg, R.B., Reynolds, B.C., Frank, M., Halliday, A.N., 2006. New sample preparation techniques for the determination
579 of Si isotopic compositions using MC-ICPMS. *Chem Geol* **235**, 95-104.

580 Gougeon, S., Kemp, K.M., Blicher, M.E., Yesson, C., 2017. Mapping and classifying the seabed of the West Greenland
581 continental shelf. *Estuarine, Coastal and Shelf Science* **187**, 231-240.

582 Grasse, P., Brzezinski, M.A., Cardinal, D., De Souza, G.F., Andersson, P., Closset, I., Cao, Z., Dai, M., Ehlert, C., Estrade,
583 N., 2017. GEOTRACES inter-calibration of the stable silicon isotope composition of dissolved silicic acid in seawater.
584 *Journal of Analytical Atomic Spectrometry* **32**, 562-578.

585 Hammond, D.E., Cummins, K.M., McManus, J., Berelson, W.M., Smith, G., Spagnoli, F., 2004. Methods for measuring
586 benthic nutrient flux on the California Margin: Comparing shipboard core incubations to in situ lander results.
587 *Limnology and Oceanography: Methods* **2**, 146-159.

588 Handmann, P., Fischer, J., Visbeck, M., Karstensen, J., Biastoch, A., Böning, C., Patara, L., 2018. The Deep Western
589 Boundary Current in the Labrador Sea From Observations and a High-Resolution Model. *Journal of Geophysical*
590 *Research: Oceans* **123**, 2829-2850.

591 Hatton, J., Hendry, K., Hawkings, J., Wadham, J., Kohler, T., Stibal, M., Beaton, A., Bagshaw, E., Telling, J., 2019.
592 Investigation of subglacial weathering under the Greenland Ice Sheet using silicon isotopes. *Geochim Cosmochim Ac*.

593 Hawkings, J.R., Hatton, J.E., Hendry, K.R., de Souza, G.F., Wadham, J.L., Ivanovic, R., Kohler, T.J., Stibal, M., Beaton, A.,
594 Lamarche-Gagnon, G., Tedstone, A., Hain, M.P., Bagshaw, E., Pike, J., Tranter, M., 2018. The silicon cycle impacted by
595 past ice sheets. *Nature Communications* **9**, 3210.

596 Hawkings, J.R., Wadham, J.L., Benning, L.G., Hendry, K.R., Tranter, M., Tedstone, A., Nienow, P., Raiswell, R., 2017. Ice
597 sheets as a missing source of silica to the polar oceans. *Nature Communications* **8**, 14198.

598 Hendry, K.R., 2017. RRS Discovery Cruise DY081, July 6th – August 8th 2017, National Marine Facilities.

599 Hendry, K.R., Cassarino, L., Bates, S.L., Culwick, T., Frost, M., Goodwin, C., Howell, K.L., 2019a. Silicon isotopic
600 systematics of deep-sea sponge grounds in the North Atlantic. *Quaternary Sci Rev* **210**, 1-14.

601 Hendry, K.R., Gong, X., Knorr, G., Pike, J., Hall, I.R., 2016. Deglacial diatom production in the tropical North Atlantic
602 driven by enhanced silicic acid supply. *Earth Planet Sc Lett* **438**, 122-129.

Hendry, K.R., Huvenne, V.A.I., Robinson, L.F., Annett, A., Badger, M., Jacobel, A.W., Ng, H.C., Opher, J., Pickering, R.A., Taylor, M.L., Bates, S.L., Cooper, A., Cushman, G.G., Goodwin, C., Hoy, S., Rowland, G., Samperiz, A., Williams, J.A., Achterberg, E.P., Arrowsmith, C., Brearley, J.A., Henley, S.F., Krause, J.W., Leng, M.J., Li, T., McManus, J.F., Meredith, M.P., Perkins, R., Woodward, E.M.S., 2019b. The biogeochemical impact of glacial meltwater from Southwest Greenland. *Progress in Oceanography*, 102126.

Hendry, K.R., Robinson, L.F., 2012. The relationship between silicon isotope fractionation in sponges and silicic acid concentration: Modern and core-top studies of biogenic opal. *Geochim Cosmochim Ac* **81**, 1-12.

Hughes, H.J., Delvigne, C., Korntheuer, M., de Jong, J., André, L., Cardinal, D., 2011. Controlling the mass bias introduced by anionic and organic matrices in silicon isotopic measurements by MC-ICP-MS. *Journal of analytical atomic spectrometry* **26**, 1892-1896.

Hvid Ribergaard, M., Anker Pedersen, S., Ådlandsvik, B., Kliem, N., 2004. Modelling the ocean circulation on the West Greenland shelf with special emphasis on northern shrimp recruitment. *Continental Shelf Research* **24**, 1505-1519.

Hydes, D.J., Aoyama, M., Aminot, A., Bakker, K., Becker, S., Coverly, S., Daniel, A., Dickson, A.G., Grosso, O., Kerouel, R., 2010. Recommendations for the determination of nutrients in seawater to high levels of precision and inter-comparability using continuous flow analysers. GO-SHIP (Unesco/IOC).

Janssen, F., Huettel, M., Witte, U., 2005. Pore-water advection and solute fluxes in permeable marine sediments (II): Benthic respiration at three sandy sites with different permeabilities (German Bight, North Sea). *Limnol Oceanogr* **50**, 779-792.

Knefelkamp, B., Carstens, K., Wiltshire, K.H., 2007. Comparison of different filter types on chlorophyll-a retention and nutrient measurements. *Journal of Experimental Marine Biology and Ecology* **345**, 61-70.

López-Acosta, M., Leynaert, A., Grall, J., Maldonado, M., 2018. Silicon consumption kinetics by marine sponges: An assessment of their role at the ecosystem level. *Limnol Oceanogr* **63**, 2508-2522.

Maldonado, M., Carmona, M.C., Velásquez, Z., Puig, A., Cruzado, A., López, A., Young, C.M., 2005. Siliceous sponges as a silicon sink: An overlooked aspect of benthopelagic coupling in the marine silicon cycle. *Limnol Oceanogr* **50**, 799-809.

März, C., Meinhardt, A.K., Schnetger, B., Brumsack, H.J., 2015. Silica diagenesis and benthic fluxes in the Arctic Ocean. *Mar Chem* **171**, 1-9.

McManus, J., Hammond, D.E., Berelson, W.M., Kilgore, T.E., Demaster, D.J., Ragueneau, O.G., Collier, R.W., 1995. Early diagenesis of biogenic opal: Dissolution rates, kinetics, and paleoceanographic implications. *Deep Sea Research Part II: Topical Studies in Oceanography* **42**, 871-903.

Meire, L., Meire, P., Struyf, E., Krawczyk, D.W., Arendt, K.E., Yde, J.C., Juul Pedersen, T., Hopwood, M.J., Rysgaard, S., Meysman, F.J.R., 2016. High export of dissolved silica from the Greenland Ice Sheet. *Geophys Res Lett* **43**, 9173-9182.

Michalopoulos, P., Aller, R.C., 2004. Early diagenesis of biogenic silica in the Amazon delta: alteration, authigenic clay formation, and storage. *Geochim Cosmochim Ac* **68**, 1061-1085.

Murillo, F.J., Kenchington, E., Tompkins, G., Beazley, L., Baker, E., Knudby, A., Walkusz, W., 2018. Sponge assemblages and predicted archetypes in the eastern Canadian Arctic. *Marine Ecology Progress Series* **597**, 115-135.

Nelson, D.M., Tréguer, P., Brzezinski, M.A., Leynaert, A., Quéguiner, B., 1995. Production and dissolution of biogenic silica in the ocean: Revised global estimates, comparison with regional data and relationship to biogenic sedimentation. *Global Biogeochem Cy* **9**, 359-372.

Olsen, A., Key, R.M., van Heuven, S., Lauvset, S.K., Velo, A., Lin, X., Schirnick, C., Kozyr, A., Tanhua, T., Hoppema, M., Jutterström, S., Steinfeldt, R., Jeansson, E., Ishii, M., Pérez, F.F., Suzuki, T., 2016. The Global Ocean Data Analysis Project version 2 (GLODAPv2) – an internally consistent data product for the world ocean. *Earth Syst. Sci. Data* **8**, 297-323.

646 Rebreanu, L., Vanderborght, J.-P., Chou, L., 2008. The diffusion coefficient of dissolved silica revisited. *Mar Chem* **112**,
647 230-233.

648 Reynolds, B.C., Aggarwal, J., Andre, L., Baxter, D., Beucher, C., Brzezinski, M.A., Engström, E., Georg, R.B., Land, M.,
649 Leng, M.J., 2007. An inter-laboratory comparison of Si isotope reference materials. *Journal of Analytical Atomic*
650 *Spectrometry* **22**, 561-568.

651 Schlitzer, R., 2012. Ocean Data View.

652 Schulz, H.D., Zabel, M., 2006. Marine geochemistry. Springer.

653 Souza, G.F., Reynolds, B.C., Rickli, J., Frank, M., Saito, M.A., Gerringa, L.J., Bourdon, B., 2012. Southern Ocean control
654 of silicon stable isotope distribution in the deep Atlantic Ocean. *Global Biogeochem Cy* **26**.

655 Strickland, J.D.H., Parsons, T.R., 1968. A practical handbook of seawater analysis. *Bull. Fish. Res. Bd. Canada* **167**, 81-
656 86.

657 Sutton, J.N., André, L., Cardinal, D., Conley, D.J., De Souza, G.F., Dean, J., Dodd, J., Ehlert, C., Ellwood, M.J., Frings, P.J.,
658 2018. A review of the stable isotope bio-geochemistry of the global silicon cycle and its associated trace elements.
659 *Frontiers in Earth Science* **5**, 112.

660 Tréguer, P.J., De La Rocha, C.L., 2013. The world ocean silica cycle. *Annual review of marine science* **5**, 477-501.

661 Varela, D.E., Brzezinski, M.A., Beucher, C.P., Jones, J.L., Giesbrecht, K.E., Lansard, B., Mucci, A., 2016. Heavy silicon
662 isotopic composition of silicic acid and biogenic silica in Arctic waters over the Beaufort shelf and the Canada Basin.
663 *Global Biogeochem Cy* **30**, 804-824.

664 Weatherall, P., Marks, K.M., Jakobsson, M., Schmitt, T., Tani, S., Arndt, J.E., Rovere, M., Chayes, D., Ferrini, V., Wigley,
665 R., 2015. A new digital bathymetric model of the world's oceans. *Earth and Space Science* **2**, 331-345.

666 Woodward, E.M.S., Rees, A.P., 2001. Nutrient distributions in an anticyclonic eddy in the northeast Atlantic Ocean,
667 with reference to nanomolar ammonium concentrations. *Deep Sea Research Part II: Topical Studies in Oceanography*
668 **48**, 775-793.

669

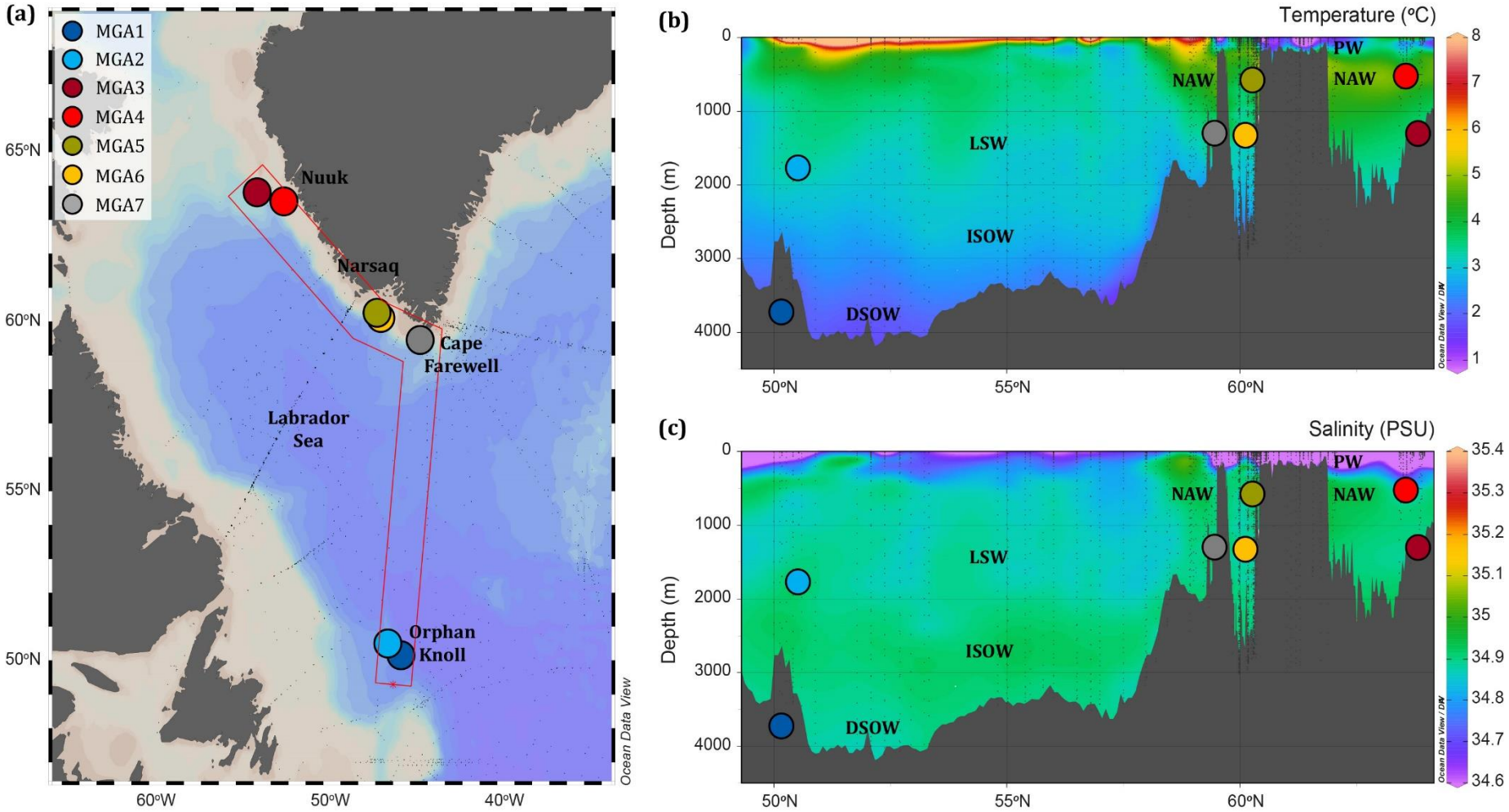

Figure 1. Locations of mega cores in this study. **(a)** Site map. Red line drawn on the map defines the boundary of the depth sections. Depth sections of **(b)** temperature and **(c)** salinity, showing the major water masses on the Greenland margin and in the Labrador Sea: Polar Water (PW), North Atlantic Water (NAW), Labrador Sea Water (LSW), Iceland-Scotland Overflow Water (ISOW), and Denmark Strait Overflow Water (DSOW). The temperature and salinity data (black dots) include new measurements from the DY081 cruise (Hendry et al., 2019b), and existing ones from the GLODAPv2 database (Olsen et al., 2016), which were interpolated in colour employing the DIVA method, an in-built function in ODV (Schlitzer, 2012). Bathymetry shown in dark grey is from GEBCO 30 arc-second grid (Weatherall et al., 2015), and sites may appear to be 'below' or 'floating above' the seafloor because they are superimposed on a representative section across the Atlantic, rather than the overlying bathymetry measured at the actual sites. The figure was generated using the ODV program (Schlitzer, 2012).

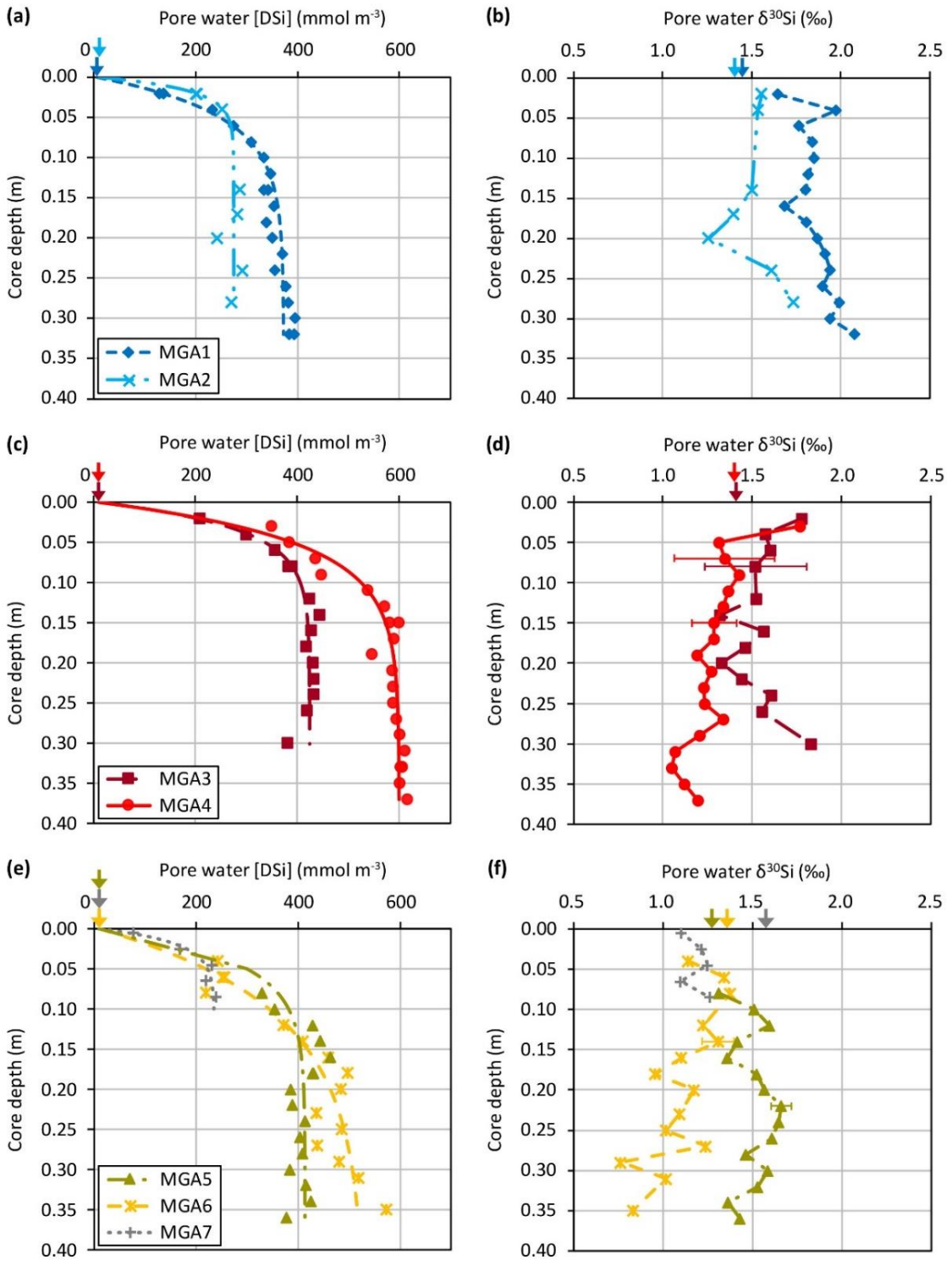

Figure 2. Pore water [DSi] and δ^{30}Si results. The mega cores are grouped together based on the geographical regions: Labrador Sea MGA1 and MGA2 **(a)** [DSi] and **(b)** δ^{30}Si profiles; West Greenland margin MGA3 and MGA4 **(c)** [DSi] and **(d)** δ^{30}Si profiles; South-West Greenland margin MGA5, MGA6 and MGA7 **(e)** [DSi] and **(f)** δ^{30}Si profiles. Lines in the [DSi] plots are (least squares) exponential fitting of the data carried out using SigmaPlot (Systat Software Inc.). The arrows mark the core-top seawater [DSi] and δ^{30}Si obtained from 0.14–0.32 m height above the sediment-water interface. Horizontal error bars represent 2 SD of repeat sample δ^{30}Si measurements (n = 2–3) carried out on the following sample intervals: MGA3-0.08 m, MGA4-0.07 m, MGA4-0.15 m, MGA5-0.22 m, and MGA6-0.14 m. MGA7 has a very short sediment core length, and hence there is only pore water data down to ~0.1 m. The lack of pore water data at the top portion of MGA5 sediment core is due to a slanted core top, and hence sampling above 0.08 m core depth would mostly be extracting core-top water instead of pore water.

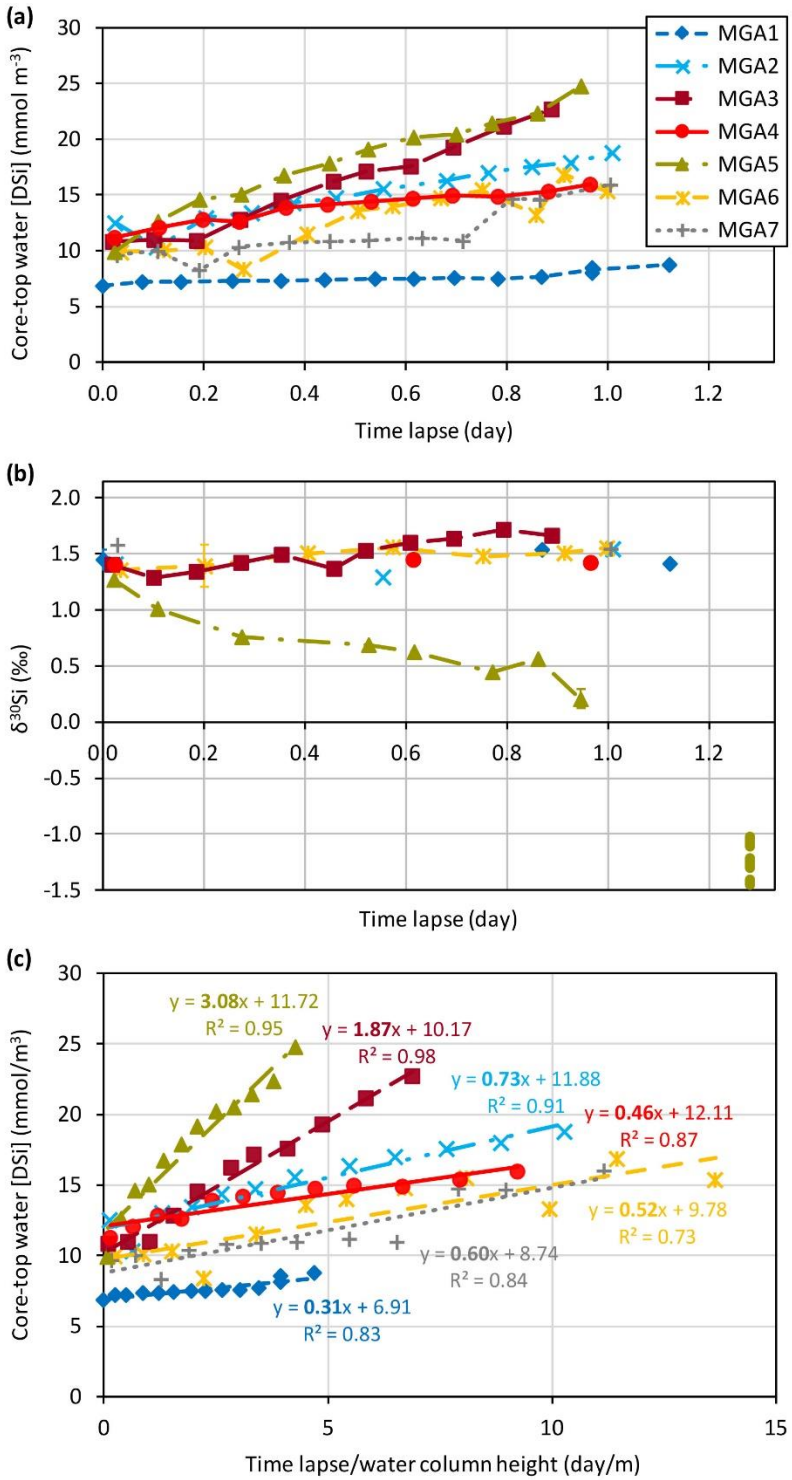

Figure 3. Core incubation results. **(a)** Core-top water [DSi], and **(b)** core-top water $\delta^{30}Si$, both against the time elapsed since the beginning of incubation. Vertical error bars represent 2 SD of repeat sample $\delta^{30}Si$ measurements (n = 2–3) carried out on the following sample intervals: MGA1-0 day, MGA3-0.19 day, MGA3-0.35 day, MGA5-0.95 day, and MGA6-0.20 day. Some of the error bars are too small to be visible in the figure. Thick dashed vertical bars at the right of the plot indicate $\delta^{30}Si$ range of sponges found atop the sediment column of MGA5. **(c)** Linear regressions of core-top water [DSi] against the ratio of incubation time to water column height. The slopes of the lines (bold text) are the apparent total benthic Si fluxes in the core incubations. All the linear regressions have p-values of less than 0.05, justifying the use of a linear model to describe the relationship above.

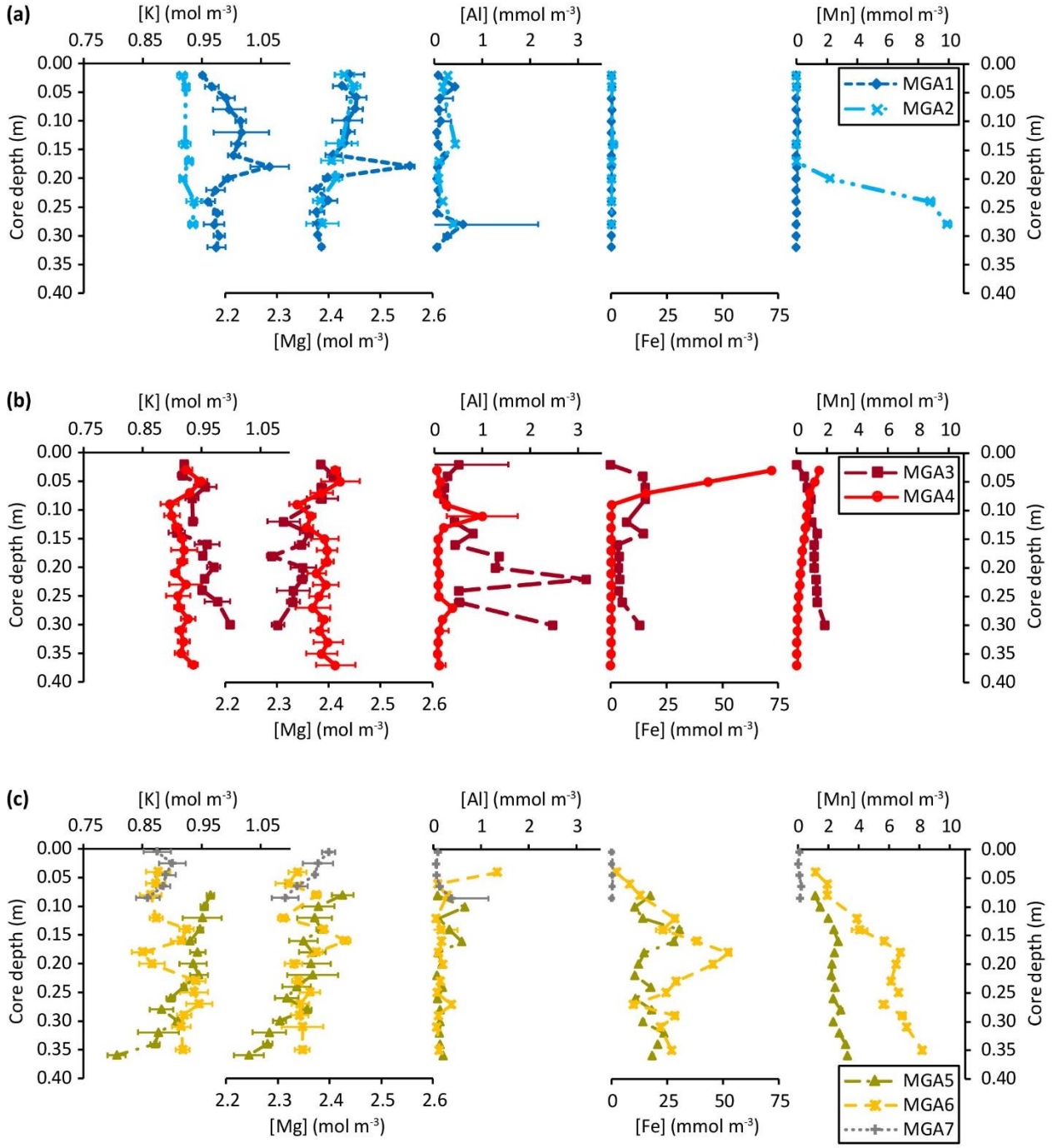

Figure 4. Pore water dissolved concentrations of major elements: [K], [Mg] and trace elements: [Al], [Fe], [Mn]. Element concentration profiles of **(a)** MGA1 and MGA2 from the Labrador Sea, **(b)** MGA3 and MGA4 from West Greenland margin, **(c)** MGA5, MGA6 and MGA7 from South-West Greenland margin. Horizontal error bars represent 2 SD analytical uncertainties, some of them are too small to be visible in the figure.

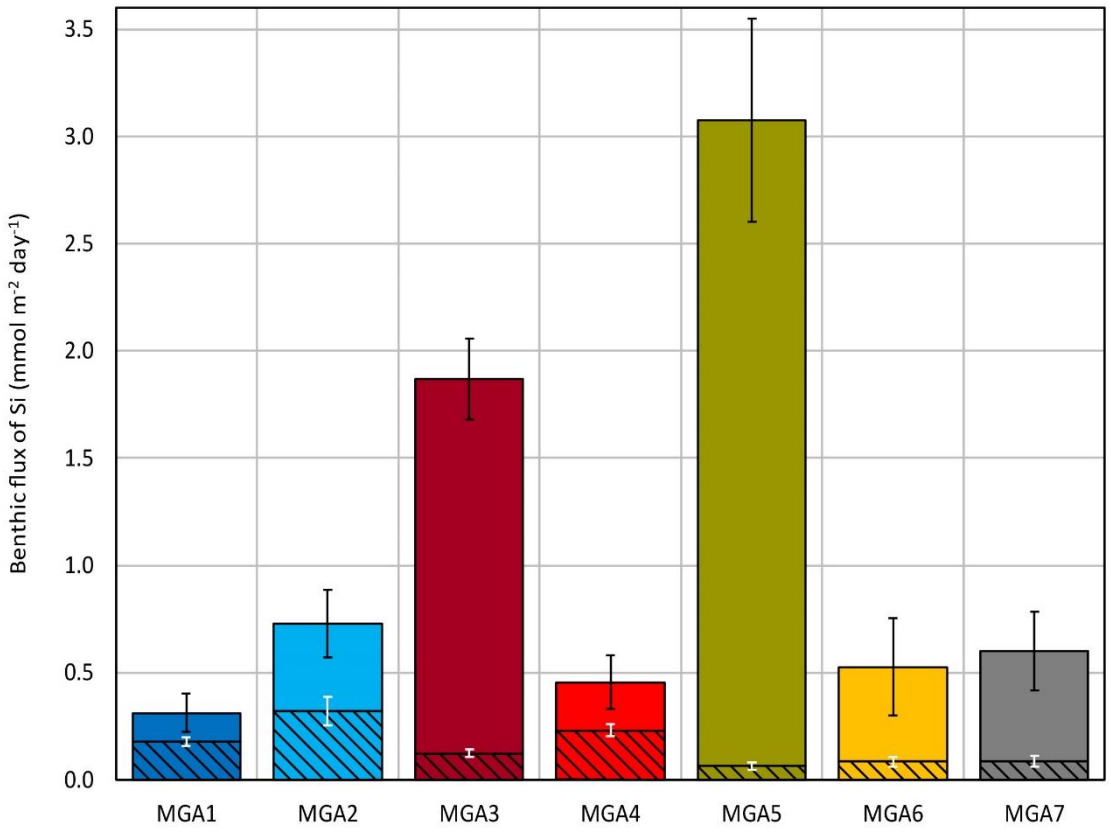

Figure 5. Benthic fluxes of Si at the study sites MGA1–MGA7. The entire lengths of the vertical columns represent the total benthic Si fluxes, J_{total}, measured from the core incubation experiments; while the hashed portion of the vertical columns denotes the benthic Si fluxes by molecular diffusion, $J_{diffusion}$, calculated from the pore water [DSi] profiles. The black and white error bars indicate the 95 % confidence intervals of J_{total} and $J_{diffusion}$ respectively.

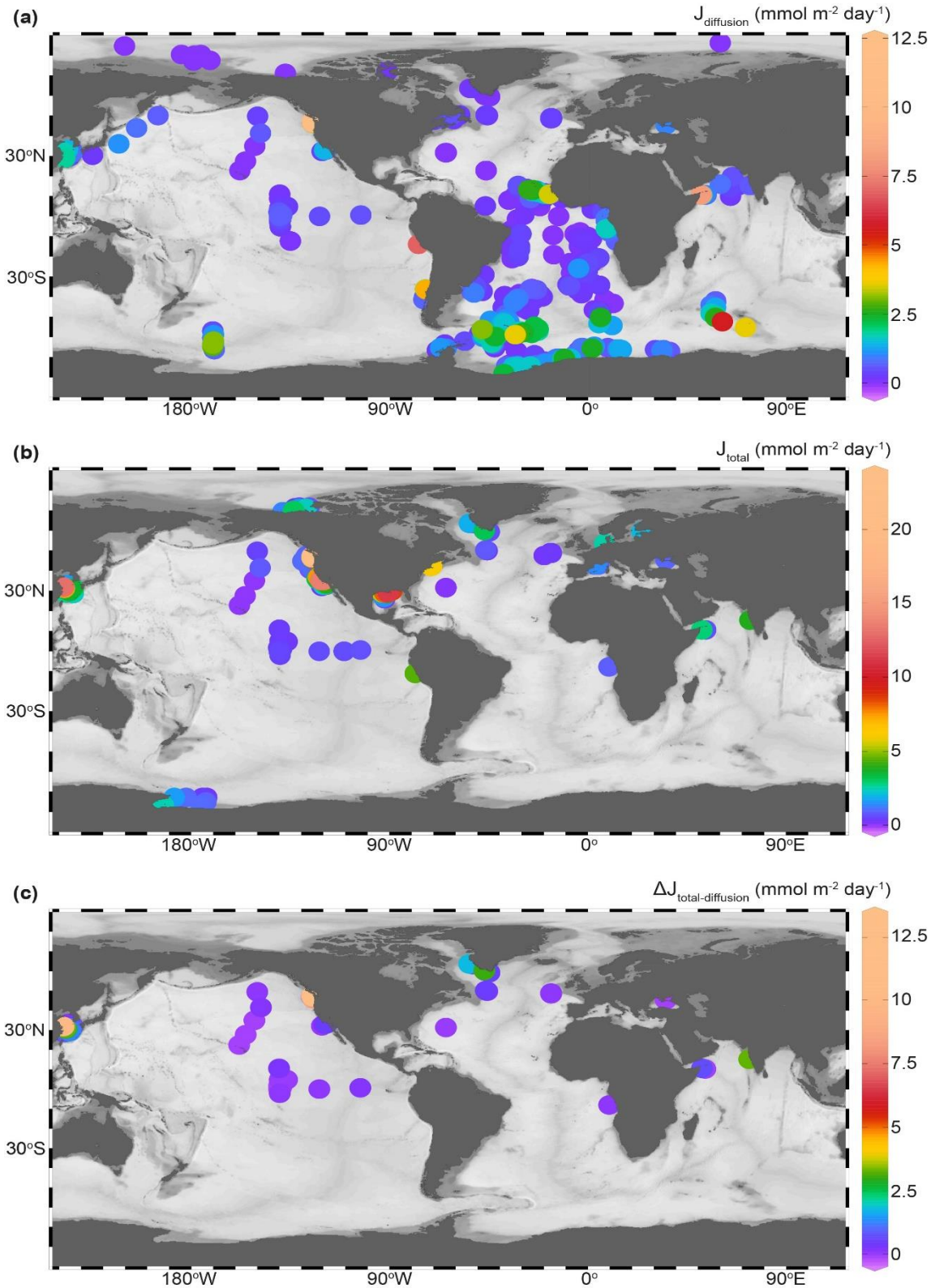

Figure 6. Compilation of global benthic Si flux data. **(a)** Diffusive benthic Si fluxes, $J_{diffusion}$, derived from pore water [DSi] profiles; **(b)** Apparent total benthic Si fluxes, J_{total}, measured using the in-situ benthic chamber method, or the laboratory core incubation method; **(c)** Differences between J_{total} and $J_{diffusion}$, $\Delta J_{total-diffusion}$. Data are plotted as circles with colour maps defined by the legends, and full references for the compiled data are listed in Appendix Table A.1. There are some differences in the magnitude of $J_{diffusion}$ between our compilation in plot (a), and that in (Frings, 2017), as they have carried out a revaluation of the compiled $J_{diffusion}$ while we keep the original values presented in previous studies. However, the difference above does

not undermine the main observations discussed in the paper. The figure was generated using the ODV program (Schlitzer, 2012).

721 **Table 1.** Study site information and sediment core description.

Core name	Site	Latitude (°N)	Longitude (°E)	Water depth (m)	Date of sampling	Basic sediment core log
DY081-MGA1	Labrador Sea	50.1592	-45.5083	3721	8 July 2017	0 – 0.4 m: greyish yellow sandy clay. Abundant foraminifera. Low bioturbation. Trace amount of very fine pebbles.
DY081-MGA2	Labrador Sea (Orphan Knoll seamount)	50.5155	-46.2790	1770	11 July 2017	Core top: green fluffy detritus. 0 – 0.15 m: dull yellowish brown muddy medium sand fining downwards. Abundant foraminifera. 0.15 – 0.38 m: yellowish brown mud. No obvious bioturbation. Small amount of fine angular pebbles.
DY081-MGA3	South West Greenland margin (off Nuuk)	63.8154	-53.7743	1301	17 July 2017	0 – 0.37 m: greyish brown muddy fine sand. Moderate bioturbation.
DY081-MGA4	South West Greenland margin (off Nuuk)	63.5530	-52.2251	519	24 July 2017	0 – 0.41 m: greyish olive mud. Low bioturbation. Strong rotten egg smell.
DY081-MGA5	South Greenland margin (off Narsaq)	60.2618	-46.8908	572	27 July 2017	Core top: diverse biology (sponges attached to coarse pebbles atop the sediment column, bivalves, annelid, shrimps). 0 – 0.10 m: grey pebbly sandy mud. Moderate bioturbation. 0.10 – 0.37 m: grey muddy clay. Low bioturbation.
DY081-MGA6	South Greenland margin (off Narsaq)	60.1160	-46.6635	1327	28 July 2017	Core top: fluffy detritus. 0 – 0.38 m: grey sandy silt. Moderate abundance of shell fragments. Low bioturbation.
DY081-MGA7	South Greenland margin (off Cape Farewell)	59.4564	-44.4151	1292	30 July 2017	Core top: green fluffy detritus, shell fragments. 0 – 0.16 m: yellowish grey sandy mud. Low bioturbation.

722

723 **Table 2.** Comparison of reference standard Si isotope composition measured in this study with published values. Measured values are long-term averages of
724 repeat analysis of the standards over the duration of this study (September 2017–October 2018).

Reference standard	Number of replicate measurements	Measured value (‰)		Published value (‰)		Reference
		$\delta^{30}Si$	2 SD	$\delta^{30}Si$	2 SD	
Diatomite	28	+1.23	0.12	+1.26	0.20	(Reynolds et al., 2007)
LMG08 sponge	26	-3.47	0.10	-3.43	0.15	(Hendry and Robinson, 2012)
$ALOHA_{1000}$ seawater	10	+1.17	0.17	+1.24	0.20	(Grasse et al., 2017)

725

Table 3. List of parameters used to estimate the diffusion Si flux, $J_{diffusion}$, at the sediment-water interface. Definition: ϕ_0 – core-top sediment porosity, θ^2 – tortuosity, D_m – molecular diffusion coefficient for silicic acid in free solution, C_0 – ambient core-top water [DSi], C_d – asymptotic pore water [DSi], β – an expression related to the sediment depth at which pore water [DSi] reaches C_d. The uncertainty associated with $J_{diffusion}$ was calculated with standard error propagation assuming Gaussian distribution, using the following formula: $2SD_{J_{diffusion}} = \left(\frac{2SD_{\phi_0}}{\phi_0} + \frac{2SD_{D_m}}{D_m} + \frac{2SD_{\theta^2}}{\theta^2} + \frac{2SD_{\beta}}{\beta} + \left(\frac{2SD_{C_d}+2SD_{C_0}}{C_d-C_0}\right)\right) \times J_{diffusion}$

	ϕ_0 [i]	2 SD	θ^2 [ii]	2 SD	D_m (m^2 day^{-1}) [iii]	2 SD	C_0 (mmol m^{-3}) [iv]	2 SD	C_d (mmol m^{-3}) [v]	2 SD	β (m^{-1}) [v]	2 SD
MGA1	0.806	0.003	1.431	0.007	4.02×10^{-5}	1.6×10^{-6}	6.82	0.27	373.0	4.9	21.5	1.3
MGA2	0.727	0.003	1.638	0.008	4.32×10^{-5}	1.5×10^{-6}	12.49	0.50	275.2	7.5	63.6	8.3
MGA3	0.514	0.003	2.331	0.012	4.38×10^{-5}	1.5×10^{-6}	10.83	0.43	424.2	5.9	31.1	2.2
MGA4	0.713	0.003	1.677	0.008	4.49×10^{-5}	1.4×10^{-6}	11.20	0.45	599.4	8.3	20.6	1.5
MGA5	0.395	0.003	2.858	0.015	4.53×10^{-5}	1.4×10^{-6}	9.88	0.40	413.8	9.8	25.2	5.8
MGA6	0.656	0.004	1.843	0.012	4.44×10^{-5}	1.5×10^{-6}	9.88	0.40	531.1	27.7	10.2	1.6
MGA7	0.419	0.003	2.740	0.014	4.44×10^{-5}	1.5×10^{-6}	9.64	0.39	235.7	11.7	56.5	11.3

[i] ϕ_0, defined as the ratio of pore volume to total volume of sediment, was determined from weight measurement of core-top sediment sample (Schulz and Zabel, 2006).

[ii] θ^2 was calculated using the equation: $\theta^2 = 1 - \ln(\phi_0^2)$ (Boudreau, 1996).

[iii] D_m is dependent on temperature. Determination of D_m for the study sites were based on previous experimental study on D_m values at a range of temperature (Rebreanu et al., 2008), given proximal bottom water temperatures acquired from DY081 cruise expedition.

[iv] Core-top water [DSi] measurements at the beginning of MGA1–MGA7 core incubation experiments (Fig. 3) were used to define C_0, assuming there was little change in the initial [DSi] within the heights of the core-top water columns, as the samples were taken 0.14–0.32 m above the core-top sediment.

[v] C_d and β were evaluated from Equation (3) through least squares exponential fit of the pore water [DSi] profiles (Fig. 2a, c & e) with C_0 values defined above. For each core site, the exponential fit was carried out on all pore water [DSi] data (including all repeat measurements without prior averaging or weighting) using the Regression Wizard function in SigmaPlot (Systat Software Inc.).

740 **Table 4.** Benthic Si flux mass balance parameters.

Core	$\frac{d(C \cdot \delta^{30}Si_{core-top\ water})}{d(t/h)}$ (mmol m^{-2} day^{-1})	$J_{diffusion}$ (mmol m^{-2} day^{-1})	J_{sponge} (mmol m^{-2} day^{-1})	$J_{residual}$ (mmol m^{-2} day^{-1})	$\delta^{30}Si_{diffusion}$ (‰)	$\delta^{30}Si_{sponge}$ (‰)	$\delta^{30}Si_{residual}$ (‰)
MGA1	0.52	0.18	-	0.13	1.65	-	1.67
MGA2	1.12	0.32	-	0.41	1.56	-	1.53
MGA3	3.29	0.12	-	1.74	1.78	-	1.76
MGA4	0.76	0.23	-	0.22	1.77	-	1.57
MGA5	-1.79	0.06	2.53	0.48 [i]	1.31	-1.25	2.71
MGA6	0.77	0.08	-	0.44	1.14	-	1.54
MGA7	0.86	0.09	-	0.52	1.10	-	1.47

741 [i] $J_{residual}$ of MGA5 is assumed to be the average of those from proximal sites MGA6 and MGA7.